Tropospheric Precursors of Anomalous Northern Hemisphere Stratospheric Polar Vortices

CHAIM I. GARFINKEL AND DENNIS L. HARTMANN

Department of Atmospheric Science, University of Washington, Seattle, Washington

FABRIZIO SASSI*

National Center for Atmospheric Research, Boulder, Colorado

(Manuscript received 5 January 2009, in final form 9 February 2010)

ABSTRACT

Regional extratropical tropospheric variability in the North Pacific and eastern Europe is well correlated with variability in the Northern Hemisphere wintertime stratospheric polar vortex in both the ECMWF reanalysis record and in the Whole Atmosphere Community Climate Model. To explain this correlation, the link between stratospheric vertical Eliassen–Palm flux variability and tropospheric variability is analyzed. Simple reasoning shows that variability in the North Pacific and eastern Europe can deepen or flatten the wintertime tropospheric stationary waves, and in particular its wavenumber-1 and -2 components, thus providing a physical explanation for the correlation between these regions and vortex weakening. These two pathways begin to weaken the upper stratospheric vortex nearly immediately, with a peak influence apparent after a lag of some 20 days. The influence then appears to propagate downward in time, as expected from wave–mean flow interaction theory. These patterns are influenced by ENSO and October Eurasian snow cover. Perturbations in the vortex induced by the two regions add linearly. These two patterns and the quasi-biennial oscillation (QBO) are linearly related to 40% of polar vortex variability during winter in the reanalysis record.

1. Introduction

Much recent work has shown that ENSO has an effect on the polar vortex. Sassi et al. (2004) forced a general circulation model (GCM) with observed sea surface temperatures (SSTs) from 1950 to 2000 and found that the warm phase of ENSO (WENSO) leads to a significantly warmer polar stratosphere. The effect was more pronounced in late winter to early spring. Manzini et al. (2006) and García-Herrera et al. (2006) noted that ENSO's North Pacific teleconnections propagate to the stratosphere. Taguchi and Hartmann (2006) forced a GCM with perpetual January conditions under both WENSO and cold phase of ENSO (CENSO) SST conditions in the Pacific and found more sudden stratospheric warmings, more midlatitude zonal wavenumber-1 (hereafter, wave-1), and a more disturbed vortex under WENSO than CENSO conditions. Limpasuvan et al. (2005a) found that in observations, the North Pacific teleconnection typically associated with CENSO leads to vortex intensification. Garfinkel and Hartmann (2007) and Camp and Tung (2007b) demonstrated statistical significance of the ENSO effect on the polar vortex in the reanalysis record. Garfinkel and Hartmann (2008, hereafter GH08) showed that the main mechanism through which ENSO modulates the vortex is by its characteristic extratropical teleconnection, which closely resembles the Pacific–North America (PNA) pattern. In particular, GH08 showed that ENSO modifies the wave-1 geopotential height field in the troposphere in such a way that wave-1 height and Eliassen–Palm (EP) flux are increased in WENSO's characteristic teleconnection relative to CENSO's characteristic teleconnection. Ineson and Scaife (2009) find that this pathway is important for ENSO's effect on European climate. It is now well established that WENSO weakens the winter stratospheric polar vortex.

* Current affiliation: Naval Research Center, Washington D.C.

Corresponding author address: Chaim I. Garfinkel, Department of Atmospheric Science, University of Washington, Seattle, WA 98195.
E-mail: cig4@atmos.washington.edu

DOI: 10.1175/2010JCLI3010.1

A series of papers, beginning with Cohen and Entekhabi (1999), has connected October Eurasian snow cover, the Siberian high in November, and variability in the December and January polar vortex. A summary of earlier work can be found in Gong et al. (2007). Snow directly affects only the lower troposphere overlying the region of the snow anomaly, however, and the pathway through which anomalous snow cover affects the nonlocal circulation has been an open question (see Cohen et al. 2005; Limpasuvan et al. 2005b). Recently, Fletcher et al. (2009) found that the diabatic cooling from the snow causes local isentropic surfaces to dome upward. In much the same way that a mountain causes an upstream high and downstream low, the domed isentropic surfaces owing to the snow induce an upstream high (extending to Europe) and a downstream low (stretching all the way to the date line). These features, and in particular the northwestern Pacific low, propagate upward into the stratosphere. Hardiman et al. (2008) showed how details of the geographic location of the downstream low over the northwestern Pacific impact a model's ability to simulate the effect on the polar vortex of October snow. For the purposes of this article, we assume that a high upstream (extending to eastern Europe) and a low downstream (extending to the northwestern Pacific) are associated with Eurasian snow cover anomalies.

The quasi-biennial oscillation (QBO) also affects the polar vortex. Holton and Tan (1980) first noted that the zonal mean geopotential height at high latitudes is significantly lower during the westerly phase of the QBO at 50 hPa than during the easterly phase. Since then, many modeling-based studies (Hampson and Haynes 2006; Pascoe et al. 2006; Naito and Yoden 2006) and data-based studies (Ruzmaikin et al. 2005; Garfinkel and Hartmann 2007) have analyzed the effects the QBO has on the polar vortex and, at the level of detail discussed in this paper, reached similar conclusions. Although the QBO is outside the main focus of this article, we will briefly discuss it.

Our investigation will center on how tropospheric anomalies generated by ENSO or October Eurasian snow anomalies, or any other process such as blocking (Martius et al. 2009), can weaken the vortex. Section 2 introduces the data and diagnostics. Section 3 motivates section 4, which provides a physical mechanism through which tropospheric anomalies can propagate upward to the vortex. Sections 5–8 explore implications.

2. Data and diagnostic tools

The 1200 UTC data produced by the European Centre for Medium-Range Weather Forecasts is used. The 40-yr ECMWF Re-Analysis (ERA-40) dataset is used for the first 45 years (Uppala et al. 2005), and the analysis is extended by using operational ECMWF Tropical Ocean and Global Atmosphere (TOGA) analysis. All relevant data from the period September 1957 to August 2007 are included in this analysis, yielding 50 years of data. Randel et al. (2004) found that the ERA-40 data is increasingly inaccurate above 10 hPa; here we show all levels.

We also use a 126-yr simulation of the Whole Atmosphere Community Climate Model (WACCM), version 3.5, to further support results from the ECMWF data. The horizontal resolution is 1.9° latitude × 2.5° longitude with 66 levels in the vertical from the ground up to ~140 km. The physics and chemistry in the middle atmosphere are identical to version 3.0 described in Garcia et al. (2007). The tropospheric convection is upgraded compared to 3.0 to include a new treatment of the dilution of entrainment in convection (Neale et al. 2008) and of the convective momentum transport (Richter and Rasch 2008). The WACCM is run as the atmospheric component of the National Center for Atmospheric Research (NCAR) Community Climate System Model (CCSM) (Collins et al. 2006). In this configuration, the model interacts with the land, a full depth ocean (which generates an ENSO-like phenomenon), and a sea ice model. The simulation is a time-slice run with chemical composition corresponding to 1995, spectrally varying solar changes, following Marsh et al. (2007), and an imposed QBO as prescribed by the Climate–Chemistry Model (CCM) evaluation activity (data are available online at http://www.pa.op.dlr.de/CCMVal/Forcings/CCMVal_Forcings_WMO2010.html) for the World Meteorological Organization ozone assessment. The simulation used in GH08 did not have a QBO and had prescribed sea surface temperatures (and thus a prescribed ENSO). Except where indicated, the hybrid sigma/pressure vertical coordinate is converted into a pressure coordinate before any analysis is performed.

The anomalous polar cap geopotential height area averaged from 70°N poleward[1] and 3 to 30 hPa (24.5 to 40.7 km in our log$p$ scaling) is used as the index for polar vortex strength [hereafter vortex strength index (VSI)]. Anomalously low heights indicate a stronger vortex. This index is computed both for daily anomalies (the anomalies are computed as deviations from that calendar date's climatology, after a ninth-order 30-day cutoff low-pass Butterworth filter has been applied to smooth

[1] A few figures were created using 65°N as the southern latitude, which maximizes the correlation with the NAM in Baldwin and Thompson (2009); the differences were minute.

the climatology) and monthly anomalies (the anomalies are computed as deviations from that calendar month's climatology). As in GH08, the QBO is the ECMWF area-averaged zonal wind from 10°S to 10°N at 50 hPa, which closely resembles the QBO phase that most strongly affects the early winter vortex (Anstey and Shepherd 2008). The Eurasian snow cover data is from Brown (2000) for 1957 to 1997 (available online at ftp://sidads.colorado.edu/DATASETS/NOAA/G02131/time_series_sce_swe.txt) and from Rutgers University for 1967 to 2007 (available online at http://climate.rutgers.edu/snowcover/table_area.php?ui_set=1andui_sort=0). In the overlap period from 1967 to 1997 we use an equally weighted sum of the two. The correlation between our index and the index in Cohen et al. (2007) from 1966 to 2004 is 0.85. Indices of geopotential height in the troposphere will be defined in section 4. The Niño-3.4 index from the Climate Prediction Center (CPC)/National Centers for Environmental Prediction (NCEP) (available online at http://www.cpc.noaa.gov/data/indices/sstoi.indices) is used in section 8 as our ENSO index. All indices are defined such that all correlations between the various indices are positive.

Outside of sections 4a and 4c (where we discuss physical mechanisms), we compute correlations between time series. The time series exhibit autocorrelation, so the number of degrees of freedom (DOFs) used in tests for significance is less than the number of days of data available. To account for this, we compute the DOFs for each index involved in a given correlation (following Bretherton et al. 1999) and then assign the smallest DOFs of the constituent indices making up that correlation as the DOFs for that correlation.

Three diagnostics are used in section 4: EP flux diagrams, wave-1 and wave-2 height variance diagrams, and height on a pressure surface. A full description of how these are calculated is in GH08. For the EP flux, the anomaly from the zonal mean for u, T, ω, and v of the daily 1200 UTC ECMWF data is taken. The zonal Fourier cross-spectrum is used to compute the wave-1 and wave-2 components of $\overline{v'\theta'}$, $\overline{\omega'u'}$, and $\overline{v'u'}$. These covariances are then used to compute the EP flux vectors using the equations from Vallis (2006, p. 537) and Andrews et al. (1987, p. 128). For section 4a, daily anomalies are computed as deviations from that calendar date's climatology, after a ninth-order 30-day cutoff low-pass Butterworth filter has been applied to smooth the climatology. For section 4c, we create monthly anomalies as follows. A monthly average of the daily EP flux is computed for each month. The annual cycle is computed by averaging over each calendar month, and the annual cycle is then subtracted from the raw EP fluxes to produce the anomalous EP fluxes. A Monte Carlo test is used to establish significance between different composites of the anomalous EP flux. If either component of the EP flux is significantly different between the two phases, the point is shaded gray. The EP flux vectors are scaled such that plotted vectors should appear divergent when they are.

Diagrams of wave-1 and wave-2 variance of geopotential height are also shown. The power spectrum is the decomposition by wavenumber of the total variance; thus, a plot of the wave-1 or wave-2 component of the power spectrum shows the variance for each wavenumber. The wave variance, rather than the actual amplitude, is plotted because of the relationship between the total variance of the streamfunction and the EP flux for Rossby waves on a β plane with constant static stability and uniform zonal flow (see Vallis 2006, p. 300, and Andrews et al. 1987, p. 188). Like the EP flux, the wave variance is computed from the daily ECMWF data, averaged into monthly means, and then has the climatology removed. The wave variance is multiplied by the density before plotting. A Monte Carlo test is used to test for significance between different composites, and significant regions are shaded. For both EP flux diagrams and wave variance diagrams, the difference between the 20 most extreme months of each phase of a given index is plotted.

A last diagnostic used is the wave-1, wave-2, and all-wave pattern of anomalous geopotential height as compared to climatology. These are produced by regressing relevant indices against a zonal Fourier decomposition of geopotential height. This allows one to visually connect the full pattern of variability associated with a given index to the wave-1 and wave-2 pattern it sets up and to then compare the anomalies in wave 1 and wave 2 to the climatological wave 1 and wave 2. If the anomalies in tropospheric wave 1 and wave 2 on a pressure level are in (out of) phase with the climatology, we expect an increase (decrease) in EP flux and height variance.

3. Tropospheric precursors of vortex weakening

We begin by objectively searching for tropospheric anomalies well correlated with vortex weakening. To do this, we compute the difference in VSI between each day and 10 days later;[2] positive (negative) values of this index mark vortex weakening (intensification). We then take the correlation of this vortex weakening index (VWI) with the time series of daily November–February (NDJF) anomalous (i.e., deviation from the 30-day smoothed

[2] Sensitivity to the choice of 10 days, as opposed to fewer or more days, was explored without qualitatively affecting the results.

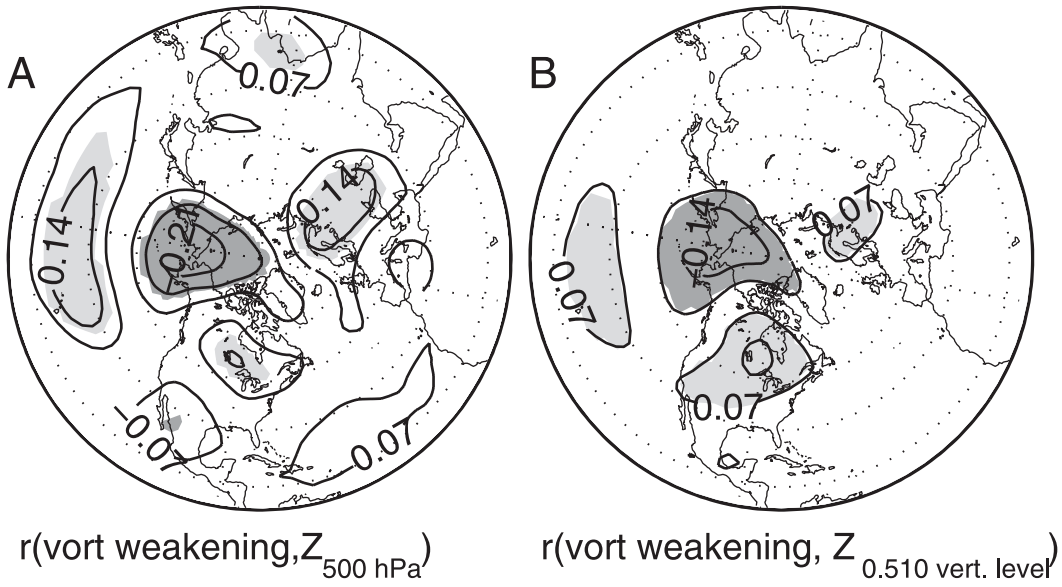

FIG. 1. Tropospheric precursors of vortex weakening: (a) correlation of 500-hPa daily anomalous heights with the vortex weakening index (the difference in VSI from day n to day $n + 10$) in NDJF in the ECMWF data and (b) identical to (a) but for the WACCM using height at the model's sigma-pressure level 0.510. Significant regions using a Student's two-tailed t test with a 95% significance level are shaded.

climatology for that day and location) geopotential height at every grid point in the midtroposphere.[3] This method pinpoints those locations in the troposphere in NDJF that were associated with a weakening or strengthening polar vortex. The tropospheric geopotential height is low-pass smoothed with a 6-day cutoff ninth-order Butterworth filter to remove synoptic variability; including synoptic variability does not qualitatively affect our results.

Figure 1a (Fig. 1b) shows the correlation of the 500-hPa (hybrid sigma-pressure level 0.510, which is near 500 hPa away from extreme topography) heights with the vortex weakening index in the reanalysis (WACCM). Three centers of a central Pacific Rossby wave train[4] and a high over eastern Europe, appear to weaken the vortex in both the model and in the reanalysis. The tropospheric influence (especially the high over eastern Europe) seems weaker in WACCM than in the reanalysis but, overall, the two agree.

These significant correlations motivate the following specific questions:

1) Can simple reasoning explain why tropospheric anomalies in these two regions would weaken the vortex? What is the time scale for this influence? Are these two regional anomalies important pathways through which ENSO and Eurasian snow cover affect the vortex? Do these regional anomalies affect the vortex more strongly in early winter or in late winter? See sections 4, 5, 6, and 7 respectively.
2) Do perturbations of the vortex associated with eastern European variability and North Pacific variability add linearly? Specifically, is the vortex at its weakest when heights over the North Pacific and eastern Europe are both in a phase that independently would act to weaken the vortex? Camp and Tung (2007a) found that the vortex was little different between easterly and westerly QBO under solar maximum conditions, and also between solar minimum and solar maximum under easterly QBO conditions; does a similar nonlinearity exist when these two tropospheric pathways are examined? See section 8.
3) Matsuno (1970) explained how planetary-scale waves in the troposphere can propagate upward and modulate the polar vortex. But the polar vortex has internally generated variability that is present even with constant tropospheric forcing (Holton and Mass 1976; Scott and Haynes 2000; Scott and Polvani 2006; Gray et al. 2003). How much of the observed variability in

[3] Looking at tropospheric geopotential height halfway through the 10-day interval, or a couple of days before the 10-day interval starts, indicates that these anomalies propagate slowly westward with time, like large-scale Rossby waves; overall, the centers found below still dominate. These centers also dominate composites of the 100 most intense vortex weakening and strengthening days.

[4] The variance of the VWI explained by the subtropical Pacific and Canadian highs in this wave train overlaps strongly with the variance of the VWI explained by the North Pacific low; in the rest of the paper, we focus on the North Pacific low exclusively.

the polar vortex is coherent with variability in the troposphere and with the QBO? See section 8.

4. Connection between regional and planetary-scale tropospheric variability

a. Our explanation

We now offer a dynamical explanation of how variability in the North Pacific and eastern Europe can affect the vortex: regional high or low height anomalies in these locations can constructively and destructively interfere with the climatological planetary waves and thus affect stratospheric EP flux. We know that the vortex is weakened climatologically by breaking planetary waves (Matsuno 1970) and that EP fluxes are proportional to the product of velocity and temperature perturbations, thus potentially quadratic in wave amplitude (Andrews et al. 1987, p. 188, 231, and Dunkerton et al. 1981). We show here that anomalies collocated with the climatological zonal asymmetries strongly affect wave-1 and wave-2 EP flux. We then search for regions that enhance both wave-1 and wave-2 EP flux and then compare these regions to the regions identified in section 3. In section 4c, we focus specifically on these regions.

Our first step is to understand how tropospheric variability affects EP flux in the lower stratosphere. Climatological zonal asymmetries in height are associated (under a series of assumptions) with wave-1 and wave-2 EP flux (see Andrews et al. 1987, p. 188, 231, and Dunkerton et al. 1981), which can propagate upward and weaken the vortex. Figures 2a and 2b show the climatological wave-1 and wave-2 components of the height field for NDJF (Fig. 2d shows the full climatological eddy height field from which the wave-1 and wave-2 components are derived). These wave-1 and wave-2 height field asymmetries, produced by the orographic and thermal forcing of the Northern Hemisphere, are linked with the EP flux that weakens the vortex in the climatology. An increase in the magnitude of these asymmetries is expected to quadratically increase EP flux. Anomalies that are in phase, and thus constructively interfere, with the climatological asymmetries are most effective in deepening them. We therefore test whether regional variability that lies in phase with, and thus enhances the magnitude of, climatological wave-1 and wave-2 height leads to increased EP flux.

We test this by creating composites of the 100 days with the most negative and most positive anomalous wave-1 (wave-2) vertical EP flux at 70 hPa (500 hPa) area averaged from 35°N and poleward in NDJF in the ECMWF data. We then examine geopotential height anomalies at 500 hPa at every gridpoint two days before the maximum in EP flux at 70 hPa (results are similar if a lag of one or three days is used) and simultaneous with the maximum in EP flux at 500 hPa. In this way, we isolate the tropospheric anomalies that typically precede wave-1 (wave-2) EP flux anomalies. We then take the difference in height field between the composite of the most negative and the most positive anomalous EP flux and plot it in Fig. 3. Figure 3 shows that wave-1 (wave-2) EP flux is significantly modulated (for the 500-hPa EP flux significance exceeds 99.99%) by a wave-1 (wave-2) pattern of extratropical height anomalies. A comparison of Fig. 3 and Figs. 2a,b shows that the tropospheric anomalies that lead to enhanced wave-1 (wave-2) EP flux are collocated with the climatological wave-1 (wave-2) zonal asymmetries. These results imply that tropospheric height anomalies that constructively interfere with the climatological planetary waves significantly affect wave-1 and wave-2 vertical EP flux in the lower stratosphere, supporting our dynamical argument.

We now return to our original question: why are North Pacific and eastern European tropospheric anomalies well correlated with vortex weakening? A close examination of Figs. 2a,b shows that climatological wave-1 and wave-2 are both low over the northwestern Pacific and high over eastern Europe; thus, anomalies that reinforce these climatological asymmetries will most likely[5] weaken the vortex. A slightly more quantitative approach is to low-pass filter the full eddy height field, in Fig. 2d, and note where highs and lows appear. We apply a ninth-order Butterworth filter with a cutoff that allows almost all wave-2 to pass through but very little wave-3 or higher to pass through to generate Fig. 2c. Climatological low wavenumber tropospheric asymmetries are strongest over the North Pacific and over eastern Europe; thus, anomalies in these locations are expected to affect the vortex.

Figure 4 is analogous to Fig. 2 but for the WACCM data. As in Fig. 2c, an enhanced low over the North Pacific will enhance tropospheric wave-1 and wave-2 heights. In Fig. 4c, the high that was more confined to eastern Europe now weakens and spreads into the Atlantic Ocean and Siberia. Thus, we might not expect the eastern European high to have quite as strong an effect in WACCM as in the reanalysis. Overall, though, WACCM has realistic tropospheric stationary waves (i.e., realistic orography and land–sea contrast). This

[5] As section 8 will show, much vortex variability is not linearly related to North Pacific and eastern European variability. In particular, variability external to these two can mask the effect of the two, and the vortex may not actually weaken even with a low over the North Pacific and a high over eastern Europe.

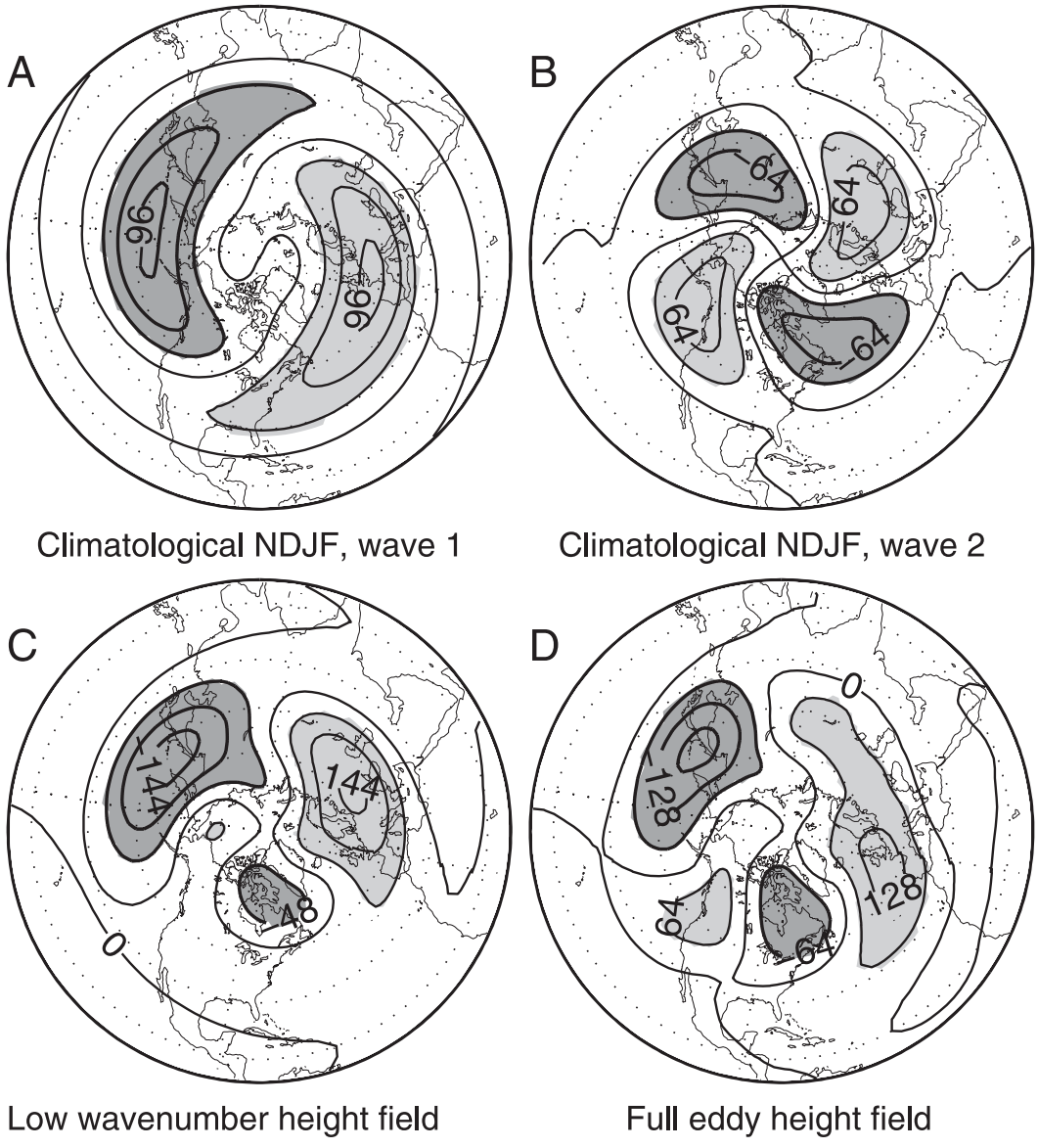

FIG. 2. Climatological (a) wave-1 and (b) wave-2 and (c) low-wavenumber and (d) all-wavenumber height fields in the ECMWF data at 500 hPa. Large anomalies are shaded to ease viewing. Contour intervals are 32 m for (a) and (b), 48 m for (c), and 64 m for (d).

similarity between the tropospheric planetary waves leads to the similarity between Figs. 3a and 3b of the regional tropospheric anomalies best correlated with weakening of the vortex.

Climatological eddies are enhanced by a low over the northern Pacific, where the climatological wave 1 and wave 2 are both low, and by a high over eastern Europe, where climatological wave 1 and wave 2 are both high. When anomalies reinforce the climatological eddies, the wave driving of the vortex from the troposphere is expected to increase. Although modeling will be necessary to explore more fully this linear interference mechanism (e.g., Smith et al. 2010, manuscript submitted to *J. Climate*) we argue that this mechanism can explain why strong anomalies in these two locations are well correlated with vortex weakening in Fig. 1.

b. The AII and EEI

Before we provide further causal evidence linking regional height variability and vortex variability, we create indices at the two locations where Figs. 1, 2c, and 4c have strong zonal asymmetries. A monthly and daily index of

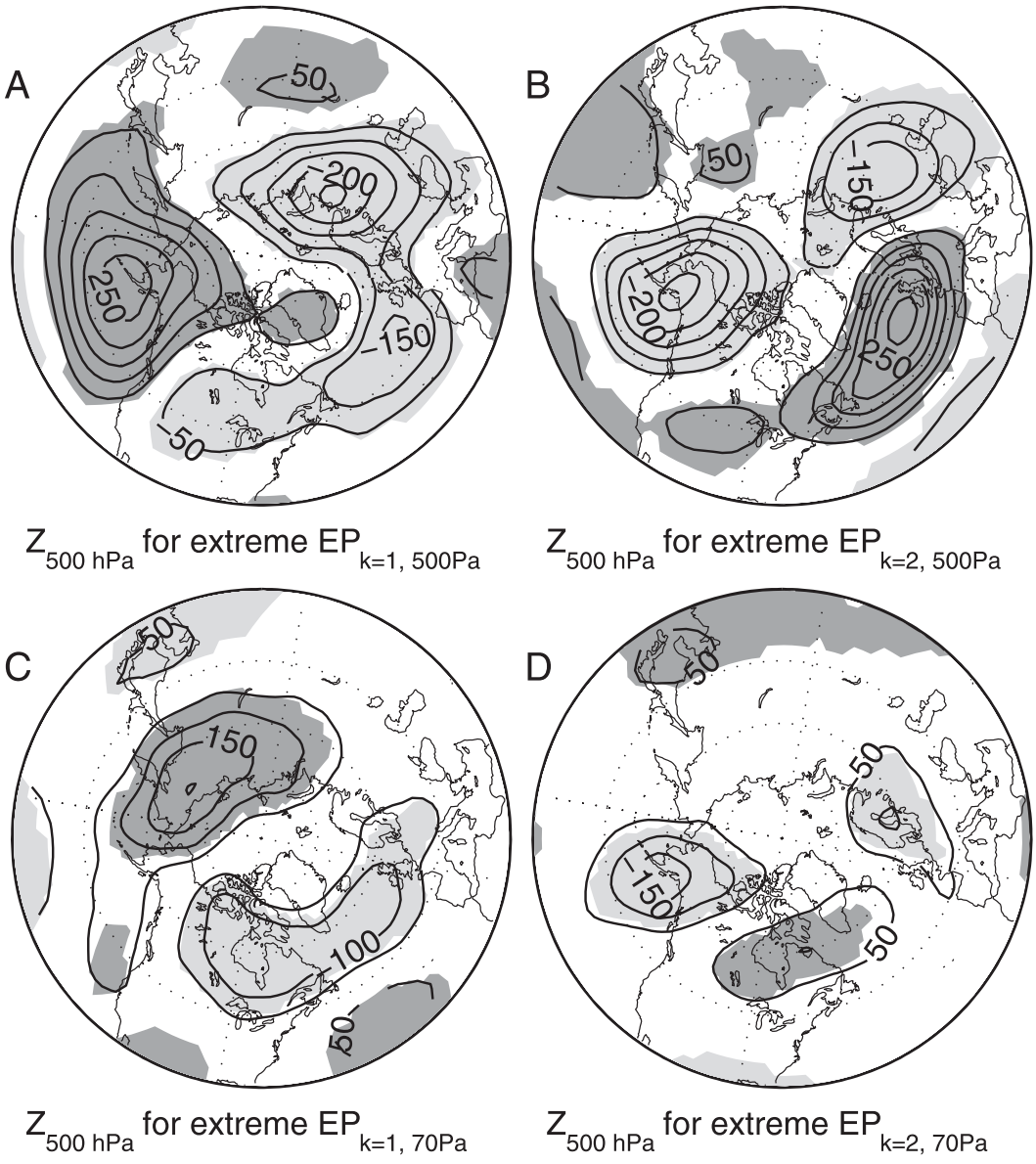

FIG. 3. Tropospheric height composited by anomalous wave-1 and wave-2 EP flux. The difference in 500-hPa daily anomalous heights between the 100 days with the most negative and positive wave-1 EP flux at (a) 500 and (c) 70 hPa. (b),(d) As in (a),(c) but for the wave-2 EP flux. Significant regions using a Student's two-tailed *t* test at the 95% significance level are shaded. No smoothing is applied to either index. To ease viewing, the lower latitude used here differs from the lower latitude used in other figures in this paper. Degrees of freedom are reduced by including all days that fall within a 5-day span as one degree of freedom. The contour interval is 50 m.

the anomalous 500-hPa geopotential height at 55°N, 175°E, hereafter the Aleutian low Index (AlI),[6] and at 60°N, 40°E, hereafter the eastern European Index (EEI), are created so as to track temporal variability at each location. Anomalies for the monthly indices are computed as deviations from that calendar month's climatology, and anomalies for the daily indices are computed as deviations from climatology after a 30-day smoother has been applied to the daily climatology. The correlation of the monthly (daily) EEI with the AlI in NDJF is −0.05 (−0.01), so the indices are independent of each other. Both indices are defined such that the positive

[6] Section 4c will discuss the precise longitudinal position for the North Pacific low that most strongly affects the vortex.

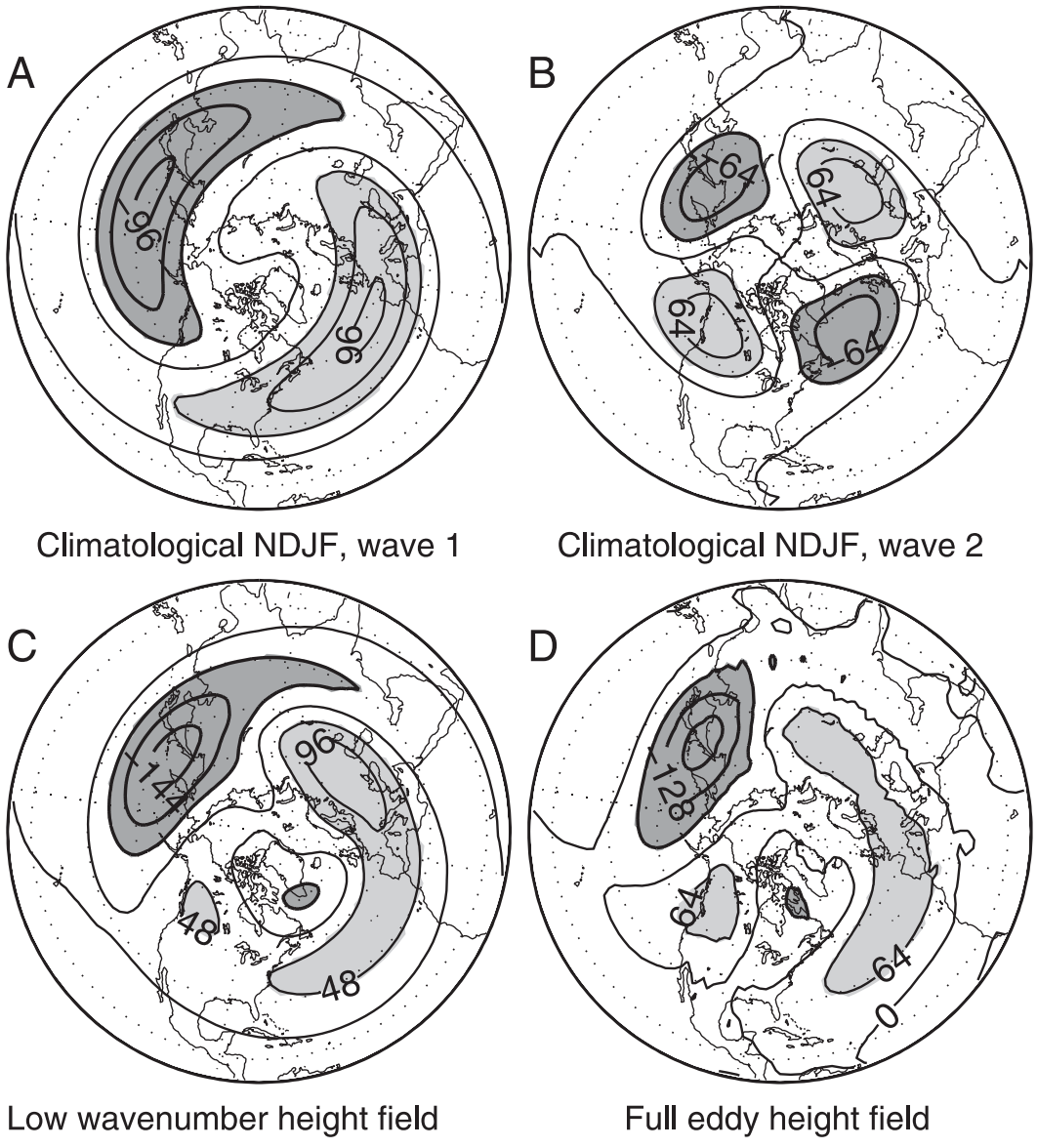

FIG. 4. As in Fig. 2 but for WACCM.

phase results in a weaker vortex. This phase is denoted the ''W'' phase; the phase that cools and strengthens the vortex is denoted the ''C'' phase.

Both AII and EEI have very low autocorrelation from month to month. For example, the lag-1 month autocorrelation of the Niño-3.4 index over the months of NDJFM is 0.97, whereas the EEI's and AII's lag-1 month autocorrelation is 0.11. These small autocorrelations mean that every month's EEI and AII is nearly statistically independent.

In GH08, the effect of the PNA on the vortex was examined. Here we focus exclusively on the North Pacific low component of the PNA because the North Pacific, more than the other centers, lies closest to a minimum (or maximum) of the climatological planetary wave pattern. The correlation of the monthly AII in NDJF with the VSI lagged one month later is 0.26, which is slightly higher than the correlation of the vortex with the PNA index as defined by the CPC/NCEP used in GH08 (0.20). The correlation between the PNA and the AII is 0.62.

c. *Mechanism for North Pacific and eastern European apparent influence*

In this subsection, we provide more causal evidence that variability of the AII and EEI leads to altered wave

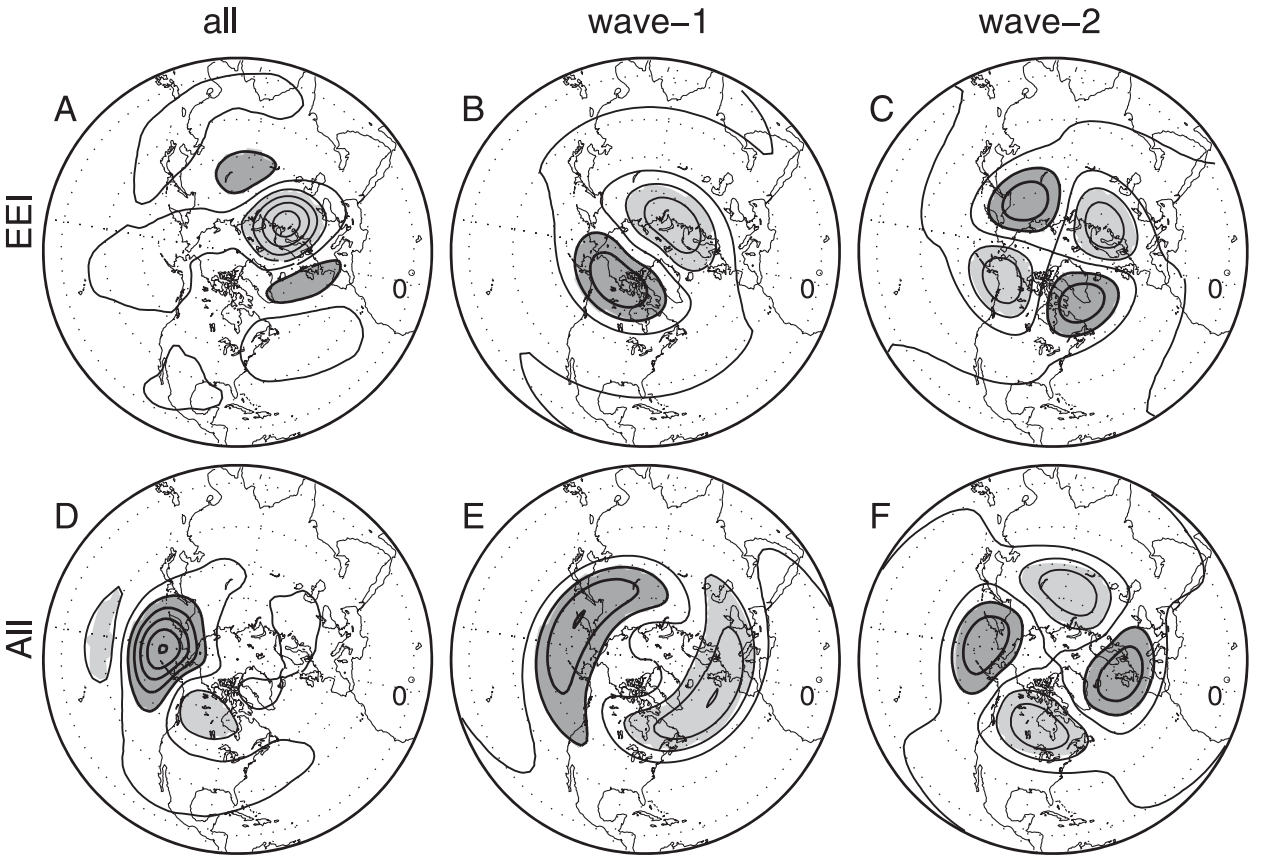

FIG. 5. Tropospheric state obtained by regressing 500-hPa heights against the (top) eastern European (60°N, 40°E) and (bottom) Aleutian (55°N, 175°E) indices: (a),(d) total (i.e., all-wave), (b),(e) wave-1, and (c),(f) wave-2 heights. Amplitudes represent a one standard deviation anomaly in height. Large anomalies are shaded to ease viewing. The last closed contour in (a) is at 80 m and in (d) at −100 m; contour intervals are (a),(d) 20 m and (b),(c),(e),(f) 10 m.

driving of the vortex. Monthly mean data are used. The first diagnostic used to study how the EEI affects the vortex is the geopotential height at 500 hPa along with its wave-1 and wave-2 components (Figs. 5a–c), as compared to climatological wave-1 and wave-2 (Figs. 2a,b). The first diagnostic is generated by regressing the EEI against the 500-hPa heights. The other diagnostics are wave-1 and wave-2 EP flux and height variance (Figs. 6a,b and 7a,b), which are obtained by calculating the difference between the 20 biggest positive and negative extremes in the EEI. The wave-1 anomaly associated with the EEI is mostly in quadrature with climatology, but wave 2 is in phase with climatology in WEEI and out of phase with climatology in CEEI. Wave-2 EP flux and height variance (Figs. 7a,b) are significantly increased in WEEI relative to CEEI, weakening the vortex. Wave 1 (Figs. 6a,b) does very little to change the vortex in WEEI relative to CEEI. We find that the net effect of an enhanced high over eastern Europe (i.e., the WEEI phase) is significantly enhanced EP flux convergence at the vortex, consistent with our physical mechanism.[7]

The second regional pathway is an Aleutian low. See Figs. 5d–f for the wave-1, wave-2, and all-wave eddy heights regressed against the AII; these are to be compared to climatological wave-1 and wave-2 (Figs. 2a,b). The wave-1 anomaly in WAII (CAII) is in phase (out of phase) with climatology. In contrast, the wave-2 anomaly is largely in quadrature with the climatological wave-2 field. Wave-1 EP flux and height variance (Figs. 6c,d) are significantly increased in WAII relative to CAII. Wave-2 EP flux and height variance (Figs. 7c,d) is significantly reduced and anomalous divergence of wave-2 EP flux occurs at the

[7] We investigated how lower stratospheric winds affect the propagation of the eastern European signal to the mid and upper stratosphere in the daily data but found no significant difference in the modulation of the vortex by eastern European variability for any of the many configurations of the lower stratospheric zonal winds examined.

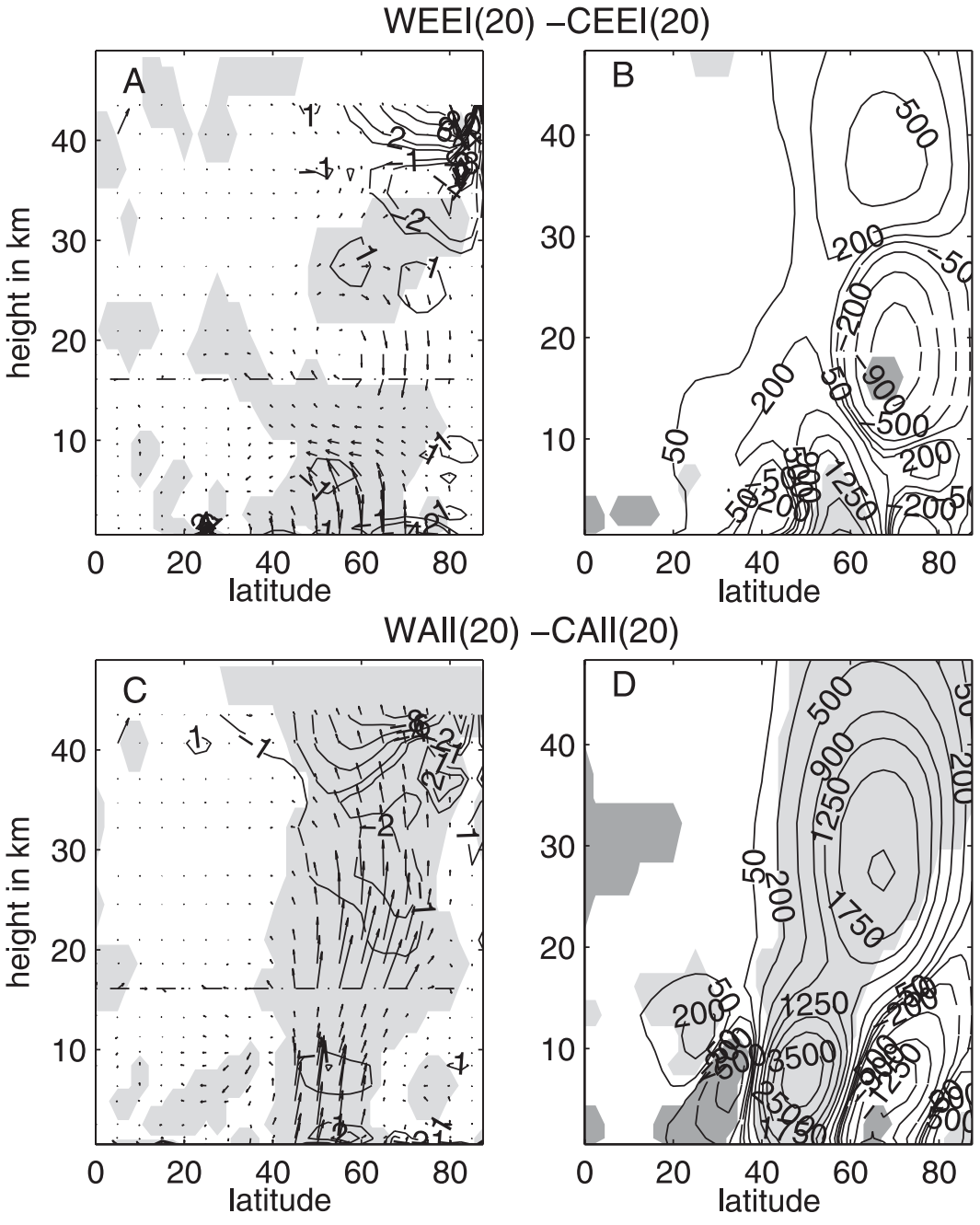

FIG. 6. Wave-1 EP flux and height variance associated with the 20 largest anomalies in the (top) eastern European and (bottom) Aleutian features. Regions with significant EP flux are shaded, the divergence of the EP flux is in units of m s^{-1} day^{-1}, and EP flux arrow lengths are multiplied by a factor of 5 above 100 hPa to be visible in the stratosphere. A reference arrow for the stratosphere is located in the top left corner of the plot; its vertical component is 1.0879×10^5 kg s^{-2} and horizontal component is 1.25×10^7 kg s^{-2}. Twenty months are in each composite. The 1-hPa and 1000-hPa levels are excluded. The height variance is in units of m^2 and has been multiplied by the basic-state density. Significantly positive (negative) regions at the 95% level are shaded light gray (dark gray).

vortex, but the wave-1 convergence overwhelms the wave-2 divergence so that total EP flux convergence at the vortex is increased in the WAII composite relative to CAII composite, also consistent with our physical mechanism.

The longitudinal position of the North Pacific low that is expected to most strongly affect the vortex in Figs. 2c and 4c differs slightly from the longitude of maximum correlation in Fig. 1. In particular, a low near the date

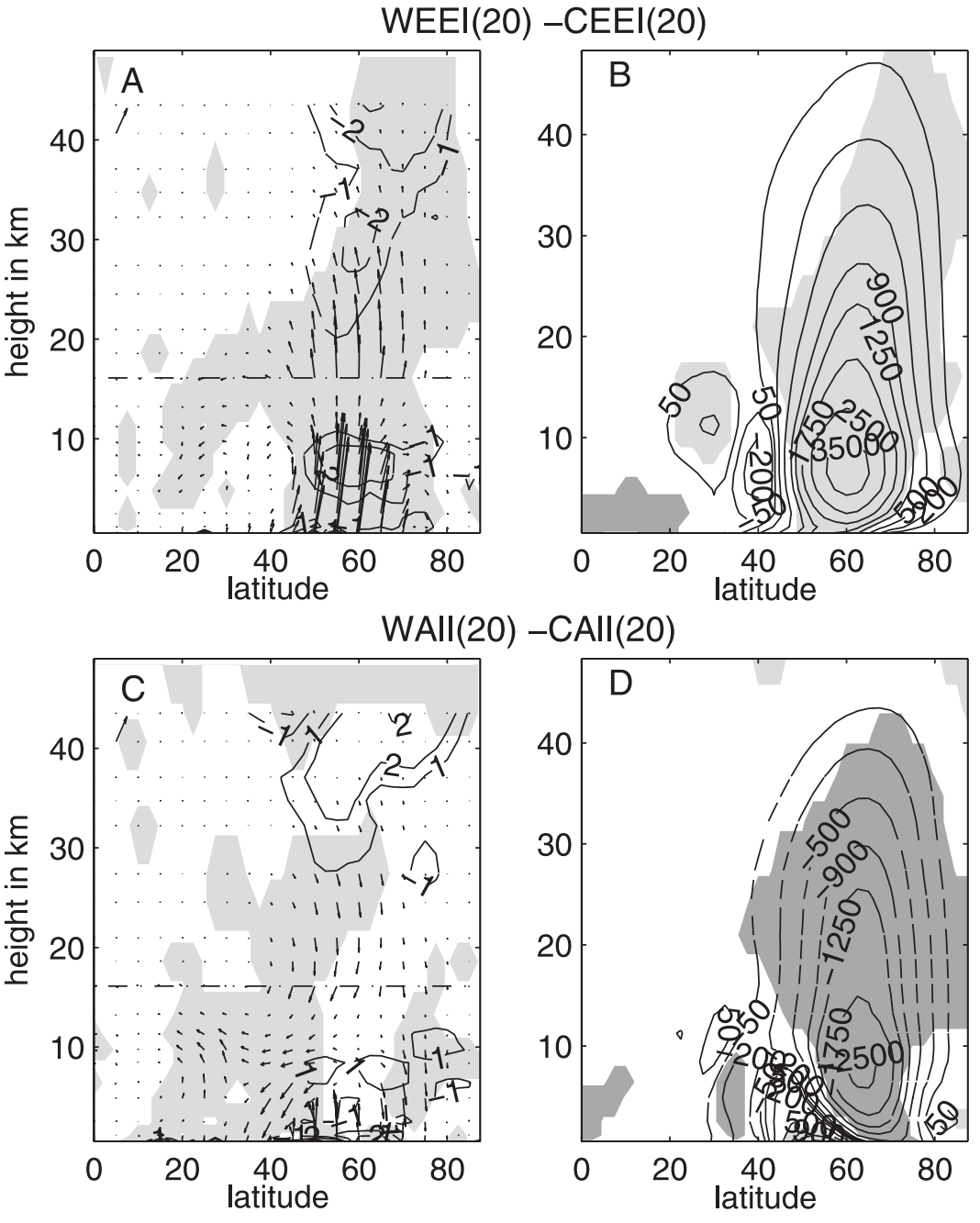

FIG. 7. As in Fig. 6 but for wave-2 EP flux and height variance.

line, not near Russia, is best correlated with vortex weakening. To study why northwestern Pacific variability has a slightly lower correlation with the vortex than Aleutian low variability, we index northwestern Pacific variability with the anomalous geopotential height at 55°N, 130°E; create the three diagnostics in Figs. 5–7 (not shown); and compare them to the same three diagnostics for the AlI. As might be expected from Figs. 2a,b, the wave-1 (wave-2) anomaly associated with a northwestern Pacific low is weaker (stronger) than for the AlI. Although wave-2 EP flux convergence at the vortex is slightly greater for an enhanced northwestern Pacific low than for the AlI, wave-1 EP flux, which substantially weakens the vortex during a deep Aleutian low, has only a moderate effect on EP flux convergence at the vortex for a northwestern Pacific low. The vortex is sensitive to the total (i.e., all-wave) EP flux convergence at the polar vortex, so a small divergence from wave 2 can be outweighed by

the very large convergence from wave 1; thus, a low over the central Pacific appears more effective in weakening in the vortex. Nonetheless, an enhanced low anywhere over the central and western North Pacific is expected to increase EP flux convergence at the vortex. Although simplified modeling will be necessary to prove that the AlI and EEI affect the vortex by constructively interfering with the climatological planetary wave field, we believe that this mechanism can explain much of the correlation in Fig. 1.

5. Time scale of vortex anomalies

Now that we have established a physical mechanism by which regional tropospheric anomalies can affect the vortex, we explore implications in the remainder of this article. In this section, we show that the EEI and AlI appear to affect the vortex in line with expectations from wave–mean flow interaction; namely, vortex anomalies grow and then appear to propagate downward with time. Because the EP flux integrated over at least a few prior weeks determines the state of the vortex at a given time (Polvani and Waugh 2004), we compute lagged correlations of the smoothed AlI and EEI with the vortex to better isolate the time scale of the wave–mean flow interaction.

The procedure is as follows. We first compute the daily EEI, AlI, QBO, and 70°N and poleward polar cap height at every level, and then smooth them with a ninth-order 30-day cutoff low-pass Butterworth filter. We then generate a daily climatology of the smoothed data and compute daily anomalies from the day's climatology. Finally, we compute the lagged correlations between the anomalous EEI, AlI, and QBO in NDJF with the anomalous vortex strength at all levels from 0 to 90 days later. In this way, we explore how anomalies in the troposphere and QBO manifest themselves as downward propagating events in the stratosphere. Because we smooth the indices, we only assign one and a half degrees of freedom per year [one and a half degrees of freedom per winter follows Bretherton et al. (1999)]. The effect of varying the cutoff on the Butterworth filter was examined, without too much qualitative effect on the results below.

Figures 8a and 8c show the lagged correlation of the vortex strength at every level with the AlI and EEI in the ECMWF data, and Fig. 8b shows the same for the AlI in the WACCM. For both AlI and EEI, the upper stratospheric polar vortex appears to weaken nearly immediately. The AlI correlation with the vortex in ECMWF peaks 20 days after the Aleutian low peaks and the peak correlation propagates downward on the time scale of a few weeks. The EEI is well correlated with the vortex some 20 days later and shows a similar downward propagation. The EEI appears to influence the lower stratospheric vortex for much longer than the AlI, but we do not understand why (the similar figure for WACCM does not show such a long-lasting influence). The QBO (see Fig. 8d) is significantly correlated with the vortex but shows no time lag as the QBO has a much longer time scale. The ostensibly downward propagation for the EEI and AlI resembles that found in Baldwin and Dunkerton (1999), Limpasuvan et al. (2004), Kuroda and Kodera (1999), and Reichler et al. (2005).

6. ENSO and October Eurasian snow

We now connect our results from section 4 with ENSO and Eurasian snow cover. Monthly mean data is used throughout.

a. ENSO

A deeper Aleutian low is part of the characteristic extratropical pattern associated with anomalous convection during WENSO (Horel and Wallace 1981; Hoskins and Karoly 1981). We now examine, in the ECMWF data, whether the Aleutian low is an important mechanism through which ENSO affects the vortex. To do this, we use regression to remove the shared variance between the AlI and the January and February VSI [$\mathrm{VSI}_{\mathrm{resid}} = \mathrm{VSI} - R_{\mathrm{AII,VSI}}\mathrm{AlI}$; January and February are the months when Sassi et al. (2004) and Manzini et al. (2006) found a maximum in the ENSO influence on the midstratosphere] and then correlate ENSO with the residual VSI. The variance of the vortex explained (in a linear sense) by ENSO drops by half once the variance associated with the Aleutian low is removed. Much of the influence of ENSO on the January and February vortex is associated with ENSO's teleconnection.

The WACCM model run also shows that an important mechanism through which ENSO modulates the vortex is the AlI. We define an ENSO index as the average temperature in the lowest sigma level over the Niño-3.4 region, and the AlI is identical to that used for the ECMWF analysis (this Niño-3.4 is correlated with WACCM's AlI at the 0.22 level). We again use regression to remove the shared variance between the AlI and the January and February VSI ($\mathrm{VSI}_{\mathrm{resid}} = \mathrm{VSI} - R_{\mathrm{AII,VSI}}\mathrm{AlI}$) and correlate ENSO with the residual VSI. The correlation drops from 0.13 to 0.04. Most of the correlation of ENSO with the January and February vortex in WACCM is due to the ENSO teleconnections. We conclude from both ECMWF and WACCM data that the Aleutian low strength is a good predictor of VSI and that ENSO contains little independent information about the vortex.

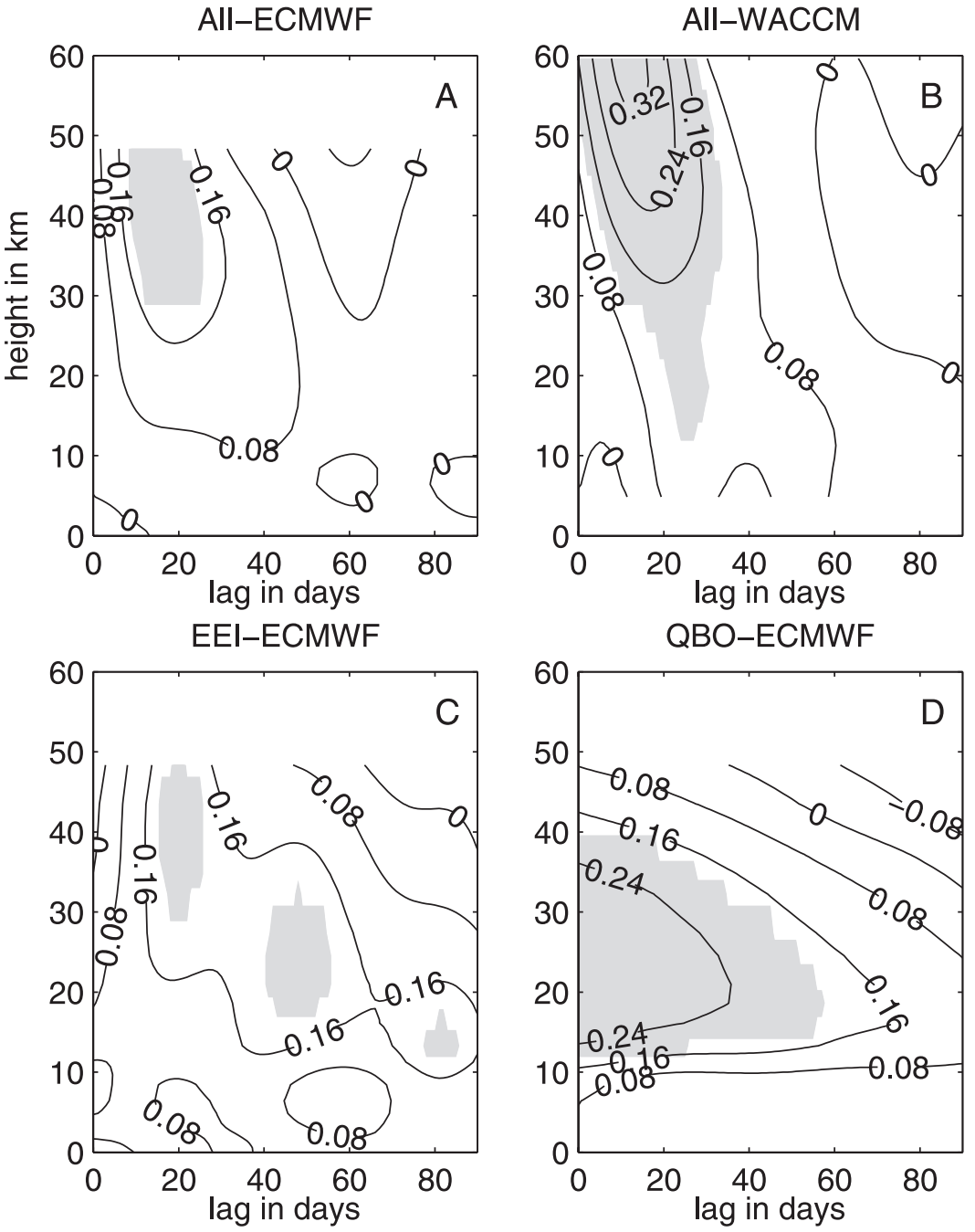

FIG. 8. Correlation of the North Pacific low (AII), QBO, and eastern European (EEI) indices in NDJF with polar cap heights lagged from 0 to 90 days later, as a function of height. Significant correlations at 95% using a one-tailed Student's *t* test are in gray. The WACCM data is plotted into the mesosphere.

b. October Eurasian snow

We now examine whether the October Eurasian snow effect on the vortex in December and January could be manifested through the EEI or the North Pacific. October Eurasian snow is not well correlated with the AII in early winter. But October Eurasian snow is well correlated with geopotential height over the northwestern Pacific (not shown, but see Fletcher et al. 2009), and the northwestern Pacific could be a conduit through which snow cover anomalies affect the vortex. Our Eurasian October snow index is significantly correlated (0.40) with the eastern European

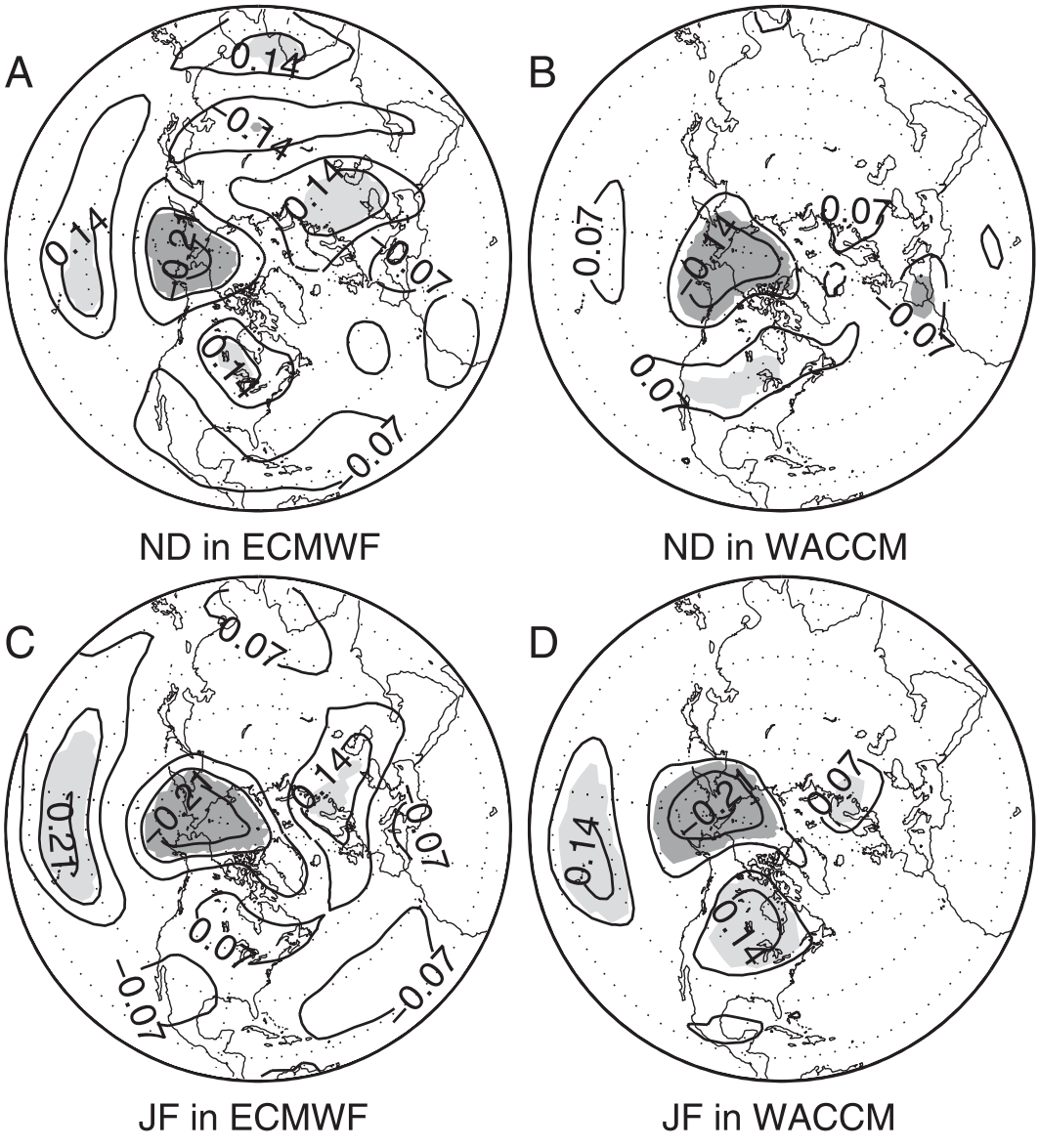

FIG. 9. As in Fig. 1 but for different halves of winter season: November–December for (a) ECMWF and (b) WACCM; January–February for (c) ECMWF and (d) WACCM.

index in November and December. Such a correlation is consistent with Cohen et al. (2001) and indicates that part of the mechanism through which October Eurasian snow might affect the polar vortex is an upstream high.

Finally, we test how much of the correlation of October Eurasian snow with the vortex is due to its coappearance with the eastern European high, the QBO, and the northwestern Pacific low. We use regression to remove the shared variance between the December QBO, EEI, and the northwestern Pacific low and the January VSI ($\mathrm{VSI}_{\mathrm{resid}} = \mathrm{VSI} - R_{\mathrm{EEI,VSI}}\mathrm{EEI} - R_{\mathrm{NWPac,VSI}}\mathrm{NWPac} - R_{\mathrm{QBO,VSI}}\mathrm{QBO}$) and correlate October Eurasian snow with the residual VSI. The correlation drops from 0.34 to 0.18 (which is no longer significant). Most of the correlation of October Eurasian snow with the January vortex is due to the presence of the QBO, EEI, and northwest Pacific low in December. By generating an upstream high and downstream low that constructively interfere with the stationary waves, October Eurasian snow anomalies appear to influence the vortex, contrary to the conclusions of Limpasuvan et al. (2005b).

7. Intrawinter variability

We now investigate whether the tropospheric anomalies best correlated with vortex anomalies change from

TABLE 1. Mean vortex weakening for nine different composites of the EEI and AII. Units are standard deviations of the vortex weakening index. The top left cell gives the mean normalized vortex weakening for the WAII/WEEI composite, the top right cell gives the vortex weakening for WAII/CEEI, etc.

	Linearity of vortex weakening		
	WEEI	No EEI	CEEI
WAII	0.43	0.07	−0.03
No AII	0.26	−0.02	−0.10
CAII	−0.11	−0.30	−0.36

TABLE 2. Correlation coefficients of wintertime indices with the VSI. The first number is the correlation between the VSI and the relevant index; the middle number, the probability at which this correlation is significantly different from zero as given by a Student's *t* test; and the last number, the degrees of freedom.

	Correlation of individual patterns with VSI		
Source	AII	QBO	EEI
ECMWF	0.46; 0.999; 47.2	0.42; 0.962; 16.0	0.27; 0.974; 47.2
WACCM	0.16; 0.962; 120.6	0.21; 0.916; 44.9	0.17; 0.975; 124.2

early to late winter. Figure 2 (the climatological zonal asymmetries) is very similar for each calendar month, and thus we do not show it for individual months. Because Fig. 2 changes so slightly between the different months, we expect that the tropospheric anomalies most strongly correlated with the VWI are the same all winter long. We test this by recreating Fig. 1 for the combination of November and December (early winter; Figs. 9a,b) and January and February (late winter; Figs. 9c,d). Although subtle differences do exist between Figs. 1 and 9, the same overall pattern, and the AII and EEI, appear.

An important caveat to our finding that early and late winter are similar needs to be mentioned. We repeated this analysis using monthly mean ECMWF data and found that the troposphere, and especially the EEI, seems more strongly related to the early to midwinter vortex than the late winter vortex.[8] We are more convinced by our results from correlating daily tropospheric data with the VWI, however, because it maximizes the degrees of freedom available from the short observational record. Thus, we find that the vortex reacts similarly to early winter and late winter tropospheric variability; as more observational data becomes available, however, this question will merit revisiting.

8. Linearity in combining the AII and EEI

We now examine whether perturbations in vortex weakening due to the AII and EEI add linearly. All days in the record are grouped into the four possible composites based on the value of the AII and EEI (the composites are WAII/WEEI, WAII/CEEI, CAII/WEEI, and CAII/CEEI; neutral days are discarded, but the composites with neutral days are included in Table 1 as they also exemplify linearity). The mean VWI is then computed for each of these four composites (see Table 1). Each of these four composites is significantly different from the other three at the 95% level except for the diagonal comparison of WEEI/CAII to CEEI/WAII. The effect of the EEI is just as significant in any AII phase, and the effect of the AII is just as significant in any EEI phase. Camp and Tung (2007a) found that the QBO and solar cycle perturbations of the vortex add nonlinearly, but for the AII and EEI we find no such nonlinearity.

Finally, we demonstrate that, on seasonal time scales, the AII, EEI, and QBO are statistically independent and covary with a significant portion of the variability of the polar vortex. We do this by computing NDJF seasonal averages of the AII, EEI, and QBO indices for each year and then correlating each index with a DJFM seasonal average of the VSI. We then compute multiple regressions of the three with the VSI. By comparing the multiple regression coefficients to the individual correlations, we can measure how statistically independent each predictor is from the other two in explaining vortex variability.

Table 2 shows the correlation coefficients. The AII, QBO, and EEI all are well correlated with the vortex. For WACCM, we also examine the difference between early winter and late winter variability for all three indices, and no intraseasonal difference is significant at the 95% level (not shown). A smaller fraction of vortex variability is correlated with these three indices in WACCM than in ECMWF, consistent with Fig. 1.

We now perform multiple regression of the AII, QBO, and EEI with the vortex. Four different multiple regressions are performed (AII/QBO, EEI/QBO, EEI/AII, and EEI/QBO/AII), and the multiple regression coefficients with the VSI for these combinations are in Table 3. The individual regression coefficients for the AII and EEI are 0.46 and 0.27. If the AII and EEI were to contain entirely independent information on the VSI, then the multiple regression coefficient would be $\sqrt{0.46^2 + 0.27^2} = 0.537$. The actual multiple regression coefficient is 0.525; this implies that AII and EEI contain

[8] In the WACCM monthly mean data, however, the troposphere's apparent impact on the early and late winter vortex is similar. The only significant difference between adjacent calendar months for either index is the difference between the effect of the AII on the March vortex relative to the February vortex.

TABLE 3. Multiple regression coefficients of seasonal indices with the VSI. The first number is the multiple correlation coefficient (minimize the squared error); the middle number, the probability that the correlation is different from zero; and the last number; the degrees of freedom.

	Multiple regression with the vortex			
Months	AII + QBO	EEI + QBO	EEI + AII	EEI + QBO + AII
All	0.63; 0.999; 16.0	0.45; 0.968; 16.0	0.53; 0.999; 47.2	0.64; 0.998; 16.0

mostly independent information about vortex state. A similar calculation can be performed for the AII and QBO; their statistical independence is even greater than that between the AII and EEI. The seasonal QBO and EEI, however, are correlated so that the multiple regression coefficient of the two is noticeably less than the maximum possible correlation. Overall, however, each of the three indices considered is fairly independent from the other two. The multiple regression coefficients suggest that 40% (0.64^2) of the total variance of the vortex is related to these three indices.

9. Conclusions

The regional tropospheric anomalies that are best correlated with vortex weakening are found to be those that are in phase with (and thus amplify the magnitude of) the climatological extratropical planetary waves, strongly suggesting (though simplified modeling work is certainly necessary) that regional anomalies that amplify the climatological stationary waves will, on average, affect the vortex. The two regional anomalies that can most effectively modulate the vortex are the North Pacific low and the eastern European high. A low over the North Pacific tends to result in a dramatic increase in wave 1 leaving the troposphere and converging at the vortex, and a high over eastern Europe tends to result in a dramatic increase in wave 2 leaving the troposphere and converging at the vortex. A low over the northwestern Pacific (possibly associated with October Eurasian snow) has a similar, but weaker, effect than that of a low over the central Pacific.

We do not mean to imply that these are the *only* possible tropospheric precursors of vortex variability. As seen in Fig. 3, high height anomalies over the northeastern Pacific (as in January 2009) can lead to anomalous wave-2 EP flux propagating up to the stratosphere and, if the wave-2 EP flux anomaly is strong enough, it can outweigh the lack of wave-1 EP flux. Similarly, a high height anomaly in the Atlantic [like that produced by the blocks in Martius et al. (2009)] can enhance wave-1 EP flux sufficiently that the loss of wave-2 is overwhelmed. Such instances are rare, though: Figs. 1 and 2 indicate that the most common way of weakening the vortex, and the most effective way of increasing the magnitude of the planetary wave pattern (i.e., the way to do it with the smallest anomaly), is to collocate an anomaly in phase with the climatological planetary wave pattern.

The tropospheric influence appears weaker in WACCM than in the reanalysis. These patterns appear to weaken the vortex in a manner consistent with the expectations from wave–mean flow interaction. In particular, an eastern European high and North Pacific low appear to weaken the upper stratospheric vortex shortly after the anomaly at the surface, and the influence seemingly propagates downward over the next month. No significant differences between early winter and late winter are apparent. The dominant pathway through which ENSO modulates the vortex is, ostensibly, its North Pacific teleconnection. Most of the variance of the polar vortex associated with October Eurasian snow can be traced back to the northwestern Pacific, QBO, and eastern Europe.

Perturbations in the vortex induced by the two pathways add linearly. Combining the QBO with the Aleutian low and the high over eastern Europe leads to a highly significant nowcaster of the polar vortex strength. Forty percent of the variance of wintertime polar vortex appears to be associated with these three sources of external variability. The remaining variance may be explained by the initial condition of the vortex, the lower stratospheric state, internal stratospheric variability, or other factors.

Acknowledgments. This work was supported by the Climate Dynamics Program of the National Science Foundation under Grant ATM 0409075. We appreciate the helpful comments from all of our reviewers.

REFERENCES

Andrews, D. G., J. R. Holton, and C. B. Leovy, 1987: *Middle Atmosphere Dynamics.* Academic Press, 489 pp.

Anstey, J. A., and T. G. Shepherd, 2008: Response of the northern stratospheric polar vortex to the seasonal alignment of QBO phase transitions. *Geophys. Res. Lett.,* **35,** L22810, doi:10.1029/2008GL035721.

Baldwin, M. P., and T. J. Dunkerton, 1999: Propagation of the Arctic Oscillation from the stratosphere to the troposphere. *J. Geophys. Res.,* **104** (D24), 30 937–30 946.

——, and D. W. J. Thompson, 2009: A simplified annular mode index based on zonal-mean data. *Quart. J. Roy. Meteor. Soc.,* **135,** 1661–1672.

Bretherton, C. S., M. Widmann, V. P. Dymnikov, J. M. Wallace, and I. Bladé, 1999: The effective number of spatial degrees of freedom of a time-varying field. *J. Climate,* **12,** 1990–2009.

Brown, R. D., 2000: Northern Hemisphere snow cover variability and change, 1915–97. *J. Climate,* **13,** 2339–2355.

Camp, C. D., and K.-K. Tung, 2007a: The influence of the solar cycle and QBO on the late winter stratospheric polar vortex. *J. Atmos. Sci.,* **64,** 1267–1283.

——, and ——, 2007b: Stratospheric polar warming by ENSO in winter: A statistical study. *Geophys. Res. Lett.,* **34,** L04809, doi:10.1029/2006GL028521.

Cohen, J., and D. Entekhabi, 1999: Eurasian snow cover variability and Northern Hemisphere climate predictability. *Geophys. Res. Lett.,* **26,** 345–348.

——, K. Saito, and D. Entekhabi, 2001: The role of the Siberian high in Northern Hemisphere climate variability. *Geophys. Res. Lett.,* **28,** 299–302.

——, D. Entekhabi, K. Saito, G. Gong, and D. Salstein, 2005: Comments on ''The life cycle of the Northern Hemisphere sudden stratospheric warmings.'' *J. Climate,* **18,** 2775–2777.

——, M. Barlow, P. J. Kushner, and K. Saito, 2007: Stratosphere–troposphere coupling and links with Eurasian land surface variability. *J. Climate,* **20,** 5335–5343.

Collins, W. D., and Coauthors, 2006: The Community Climate System Model version 3 (CCSM3). *J. Climate,* **19,** 2122–2143.

Dunkerton, T. J., C.-P. Hsu, and M. E. McIntyre, 1981: Some Eulerian and Lagrangian diagnostics for a model stratospheric warming. *J. Atmos. Sci.,* **38,** 819–844.

Fletcher, C. G., S. C. Hardiman, P. J. Kushner, and J. Cohen, 2009: The dynamical response to snow cover perturbations in a large ensemble of atmospheric GCM integrations. *J. Climate,* **22,** 1208–1222.

Garcia, R. R., D. Marsh, D. Kinnison, B. Boville, and F. Sassi, 2007: Simulation of secular trends in the middle atmosphere, 1950–2003. *J. Geophys. Res.,* **112,** D09301, doi:10.1029/2006JD007485.

García-Herrera, R., N. Calvo, R. R. Garcia, and M. A. Giorgetta, 2006: Propagation of ENSO temperature signals into the middle atmosphere: A comparison of two general circulation models and ERA-40 reanalysis data. *J. Geophys. Res.,* **111,** D06101, doi:10.1029/2005JD006061.

Garfinkel, C. I., and D. L. Hartmann, 2007: Effects of the El Niño–Southern Oscillation and the Quasi-Biennial Oscillation on polar temperatures in the stratosphere. *J. Geophys. Res.,* **112,** D19112, doi:10.1029/2007JD008481.

——, and ——, 2008: Different ENSO teleconnections and their effects on the stratospheric polar vortex. *J. Geophys. Res.,* **113,** D18114, doi:10.1029/2008JD009920.

Gong, G., J. Cohen, D. Entekhabi, and Y. Ge, 2007: Hemispheric-scale climate response to northern Eurasia land surface characteristics and snow anomalies. *Global Planet. Change,* **56,** 359–370.

Gray, L. J., S. Sparrow, M. Juckes, A. O'Neill, and D. G. Andrews, 2003: Flow regimes in the winter stratosphere of the Northern Hemisphere. *Quart. J. Roy. Meteor. Soc.,* **129,** 925–945.

Hampson, J., and P. Haynes, 2006: Influence of the equatorial QBO on the extratropical stratosphere. *J. Atmos. Sci.,* **63,** 936–951.

Hardiman, S. C., P. J. Kushner, and J. Cohen, 2008: Investigating the ability of general circulation models to capture the effects of Eurasian snow cover on winter climate. *J. Geophys. Res.,* **113,** D21123, doi:10.1029/2008JD010623.

Holton, J. R., and C. Mass, 1976: Stratospheric vacillation cycles. *J. Atmos. Sci.,* **33,** 2218–2225.

——, and H. C. Tan, 1980: The influence of the equatorial quasi-biennial oscillation on the global circulation at 50 mb. *J. Atmos. Sci.,* **37,** 2200–2208.

Horel, J. D., and J. M. Wallace, 1981: Planetary-scale atmospheric phenomena associated with the Southern Oscillation. *Mon. Wea. Rev.,* **109,** 813–829.

Hoskins, B. J., and D. Karoly, 1981: The steady linear response of a spherical atmosphere to thermal and orographic forcing. *J. Atmos. Sci.,* **38,** 1179–1196.

Ineson, S., and A. A. Scaife, 2009: The role of the stratosphere in the European climate response to El Niño. *Nat. Geosci.,* **2,** 32–36, doi:10.1038/ngeo381.

Kuroda, Y., and K. Kodera, 1999: Role of planetary waves in the stratosphere–troposphere coupled variability in the Northern Hemisphere winter. *Geophys. Res. Lett.,* **26,** 2375–2378.

Limpasuvan, V., D. W. J. Thompson, and D. L. Hartmann, 2004: The life cycle of the Northern Hemisphere sudden stratospheric warmings. *J. Climate,* **17,** 2584–2596.

——, D. L. Hartmann, D. W. J. Thompson, K. Jeev, and Y. L. Yung, 2005a: Stratosphere–troposphere evolution during polar vortex intensification. *J. Geophys. Res.,* **110,** D24101, doi:10.1029/2005JD006302.

——, D. W. J. Thompson, and D. L. Hartmann, 2005b: Reply. *J. Climate,* **18,** 2778–2780.

Manzini, E., M. A. Giorgetta, L. Kornbluth, and E. Roeckner, 2006: The influence of sea surface temperatures on the northern winter stratosphere: Ensemble simulations with the MAECHAM5 model. *J. Climate,* **19,** 3863–3881.

Marsh, D., R. R. Garcia, D. E. Kinnison, B. A. Boville, F. Sassi, S. C. Solomon, and K. Matthes, 2007: Modeling the whole atmosphere response to solar cycle changes in radiative and geomagnetic forcing. *J. Geophys. Res.,* **112,** D23306, doi:10.1029/2006JD008306.

Martius, O., L. M. Polvani, and H. C. Davies, 2009: Blocking precursors to stratospheric sudden warming events. *Geophys. Res. Lett.,* **36,** L14806, doi:10.1029/2009GL038776.

Matsuno, T., 1970: Vertical propagation of stationary planetary waves in the winter Northern Hemisphere. *J. Atmos. Sci.,* **27,** 871–883.

Naito, Y., and S. Yoden, 2006: Behavior of planetary waves before and after stratospheric sudden warming events in several phases of the equatorial QBO. *J. Atmos. Sci.,* **63,** 1637–1649.

Neale, R. B., J. H. Richter, and M. Jochum, 2008: The impact of convection on ENSO: From a delayed oscillator to a series of events. *J. Climate,* **21,** 5904–5924.

Pascoe, C. L., L. J. Gray, and A. A. Scaife, 2006: A GCM study of the influence of equatorial winds on the timing of sudden stratospheric warmings. *Geophys. Res. Lett.,* **33,** L06825, doi:10.1029/2005GL024715.

Polvani, L. M., and D. W. Waugh, 2004: Upward wave activity flux as a precursor to extreme stratospheric events and subsequent anomalous surface weather regimes. *J. Climate,* **17,** 3548–3554.

Randel, W., and Coauthors, 2004: The SPARC intercomparison of middle atmosphere climatologies. *J. Climate,* **17,** 986–1003.

Reichler, T., P. J. Kushner, and L. M. Polvani, 2005: The coupled stratosphere–troposphere response to impulsive forcing from the troposphere. *J. Atmos. Sci.,* **62,** 3337–3352.

Richter, J. H., and P. J. Rasch, 2008: Effects of convective momentum transport on the atmospheric circulation in the Community Atmosphere Model, version 3. *J. Climate,* **21,** 1487–1499.

Ruzmaikin, A., J. Feynman, X. Jiang, and Y. L. Yung, 2005: Extratropical signature of the quasi-biennial oscillation. *J. Geophys. Res.,* **110,** D11111, doi:10.1029/2004JD005382.

Sassi, F., D. Kinnison, B. A. Boville, R. R. Garcia, and R. Roble, 2004: Effect of El Niño–Southern Oscillation on the dynamical, thermal, and chemical structure of the middle atmosphere. *J. Geophys. Res.,* **109,** D17108, doi:10.1029/2003JD004434.

Scott, R. K., and P. H. Haynes, 2000: Internal vacillations in stratosphere-only models. *J. Atmos. Sci.,* **57,** 3233–3250.

——, and L. M. Polvani, 2006: Internal variability of the winter stratosphere. Part I: Time-independent forcing. *J. Atmos. Sci.,* **63,** 2758–2776.

Taguchi, M., and D. L. Hartmann, 2006: Increased occurrence of stratospheric sudden warming during El Niño as simulated by WACCM. *J. Climate,* **19,** 324–332.

Uppala, S. M., and Coauthors, 2005: The ERA-40 re-analysis. *Quart. J. Roy. Meteor. Soc.,* **131,** 2961–3012.

Vallis, G. K., 2006: *Atmospheric and Oceanic Fluid Dynamics: Fundamentals and Large-Scale Circulation*. Cambridge University Press, 745 pp.